Analysis of short circuit current loss in rear emitter crystalline Si solar cell

Tatsuro Watahiki, Yumiko Kobayashi, Takayuki Morioka, Shinya Nishimura, Daisuke Niinobe, Kunihiko Nishimura, Hidetada Tokioka, and Mikio Yamamuka
Advanced Technology R&D Center, Mitsubishi Electric Corporation, 8-1-1 Tsukaguchi-Honmachi, Amagasaki 661-8661, Hyogo, Japan

(Received 16 March 2016; accepted 7 May 2016; published online 25 May 2016)

Short circuit current (J_{sc}) loss in rear emitter crystalline Si solar cell is analyzed in detail by a 2D device simulation and compared with the experimental results. There is a significant loss in J_{sc} for the rear emitter n-Si solar cell with an n-type doped front surface field (FSF) when the base substrate resistivity is low. It is due to an increase in recombination in the FSF region led by a less barrier height for minority carriers with a lower substrate resistivity. The barrier height less than 0.1 eV causes large loss in J_{sc}. To achieve higher J_{sc} for the cells with FSF, the control of the doping concentration in FSF, the substrate thickness, and the barrier height for the minority carriers are important. A rear emitter heterojunction Si solar cell with an amorphous Si passivation layer shows no substrate resistivity dependence on J_{sc} since an amorphous Si possess a higher barrier height and a long bulk lifetime of more than a few milliseconds. [http://dx.doi.org/10.1063/1.4951003]

I. INTRODUCTION

The n-type crystalline Si solar cell possesses a potential to achieve a very high energy conversion efficiency due to a higher bulk lifetime, a larger thermal tolerance, and a less impact of metallurgical impurities on the bulk lifetime than p-type crystalline Si.[1,2] We have developed the n-type crystalline Si solar cell with PERT (Passivated Emitter Rear Totally diffused) structure and achieved an efficiency of over 21%.[3] On the other hand, a very high efficiency of over 24% is reported for a heterojunction Si solar cell.[4] In this structure, amorphous Si is introduced as a passivation layer and enables to achieve a high open circuit voltage (V_{oc}) of over 0.740 V. We have also investigated on the heterojunction Si solar cell and reached the efficiency of 23.46% with a rear emitter (RE) structure.[5] An RE Si solar cell has an emitter on the rear side of the Si substrate against the incoming sun light. This RE structure has several advantages to the front-emitter (FE) structure.[6,7] Since the emitter is located on the rear side, the emitter has less impact on the optical loss and it has more freedom for the design of structure, such as a surface morphology, a sheet resistance, and a grid pitch. In addition, the majority carrier transport (i.e., electron for n-type) is enhanced by the assistance of the Si substrate so that the grid pitch for the front side (n-doped side) can be wider without the significant increase in the series resistance. Thus, the PERT cell can reach a higher efficiency by converting to the RE structure.[8] However, the rear emitter cell with front surface field (FSF) shows less efficiency than the front emitter cell. Figure 1 shows I-V and internal quantum efficiency (IQE) curves of the bifacial solar cell that we have developed. The light was incident from either front emitter (for FE) or rear side (for RE) for the identical cell. The measurement was done with a gold stage in this case to eliminate transmittance loss. The V_{oc} and a fill factor (F.F.) were similar for both cases because these parameters were related to the passivation quality and the series resistance, which were basically related to the diode parameters under dark condition. However, the short circuit current (J_{sc}) was 1.4 mA/cm^2 lower for the RE cell than for the FE cell. Around 0.5 mA/cm^2 as a part of the difference can be explained by the difference in a grid design and a reflectance loss, but still the RE cell shows around 1 mA/cm^2 lower J_{sc} (around 0.5% point in efficiency) than the FE cell. From the IQE curves, we found that the J_{sc} loss was mainly due to the loss in the short to medium wavelength region. It suggests that J_{sc} loss was most probably due to the bulk recombination and/or recombination in n^+/n^{++} region where the auger recombination and the surface recombination (SR) occurred. However, only from the QE curves, we found it was difficult to quantify the impact of the recombination in the bulk and the surface. Therefore, we also need to consider not only J_{sc} but also other parameters for analyzing this phenomenon in detail.

There are some reports that the resistivity of the substrate has a strong influence on J_{sc}.[9,10] This is a problem especially for an n-type Si cell. A resistivity variation of the n-type Si ingot is larger than that of the p-type wafer because the phosphorus atoms have a smaller segregation coefficient in Si than boron atoms.[11] To get the benefit of RE structure, the loss in J_{sc} for the RE cell must be clarified. There are several papers which discussed about the J_{sc} loss for the RE Si solar cell,[12–16] but a detailed analysis through the calculation and the comparison with the experimental data is not yet discussed well. Therefore, the effect of the resistivity of the substrate is still ambiguous and the approach to reduce the loss in J_{sc} is unclear. In this paper, we report the comprehensive study of the RE Si solar cell with the resistivity dependence. We have performed the 2D simulation to analyze the J_{sc} loss in our RE cell and compared with the experimental results.

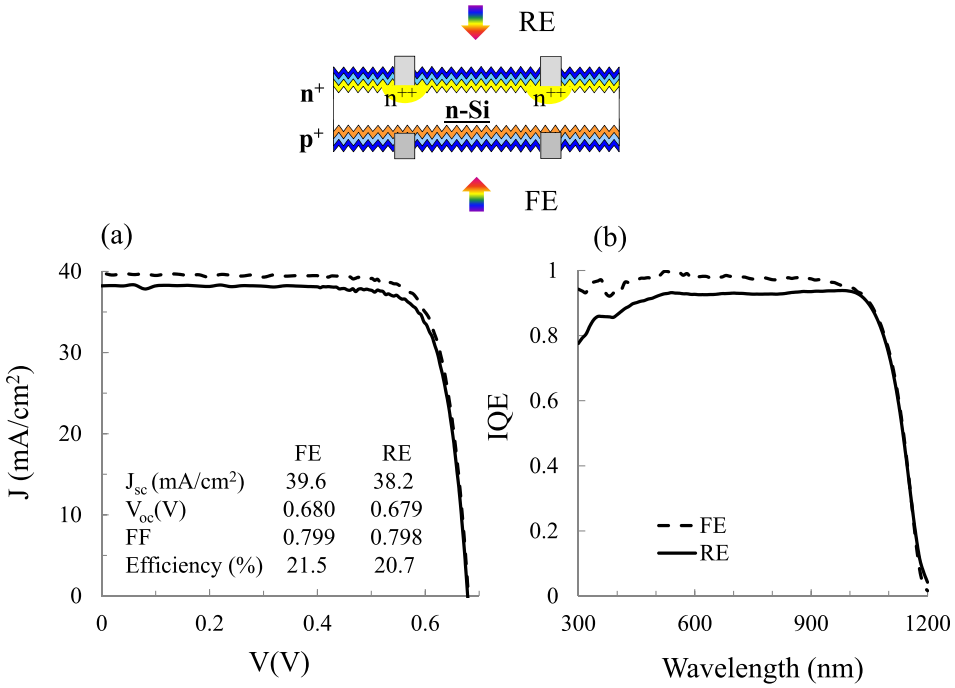

FIG. 1. (a) I-V and (b) IQE characteristics of a bifacial solar cell. The dashed line indicates the data for the front emitter cell (FE, the light enters the emitter side) and the solid line indicates the data for the rear emitter cell (RE, the light enters the substrate side).

II. EXPERIMENT

We fabricated the rear emitter n-type crystalline Si solar cell. A detailed fabrication process was similar to our FE cell, as shown in Ref. 3. The total area of the cell was 239 cm^2. We used a boron emitter fabricated by an atmospheric pressure chemical vapor deposition technique. The n^+/n^{++} selective doped regions were fabricated on the front side as a collector, using the combination of the dopant paste and the $POCl_3$ diffusion. The dopant paste was screen printed on the front side of the wafer and the dopants were thermally diffused to form n^{++} region, followed by $POCl_3$ diffusion in the same furnace to form n^+ region. Then the front surface was passivated by SiN after removing the dopant source. The silver grid electrode was printed and contacted on the n^{++} region through a firing process. The resistivity of the substrate was varied in the range of 0.55–5.6 Ω cm. I-V characteristics were measured in house using the solar simulator. The error in J_{sc} was ± 0.1 mA/cm^2.

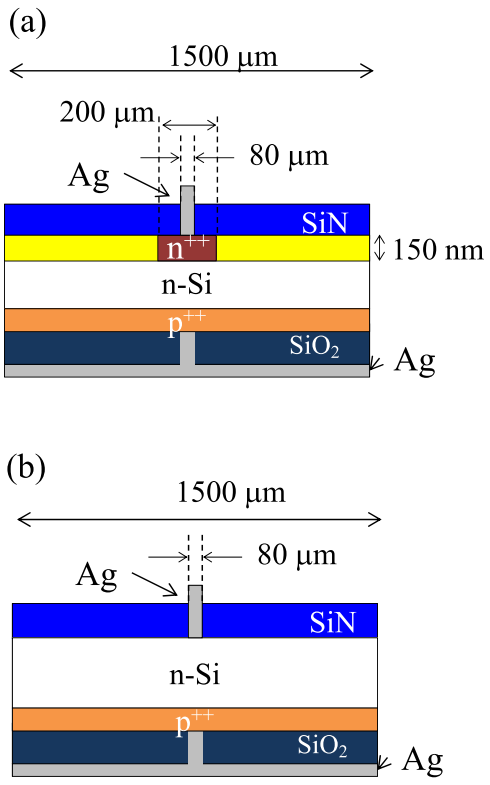

FIG. 2. Schematic structures of the rear emitter cell used for the calculation (a) with and (b) without n^+/n^{++} doping regions. For models #2 and #3, there are n^+ and n^{++} regions, which has the phosphorus doping concentration of 1×10^{19} and 5×10^{19} cm^{-3}, respectively. The width of the unit cell, the n^{++} region, and the grid are 1500 μm, 200 μm, and 80 μm, respectively. For model #1, the n-type doping region as FSF is not formed.

For the calculation of the I-V characteristics of the solar cells, we have used 2D device simulator ATLAS (Silvaco, Inc.).[17] Schematic structures of the RE cell for the calculation models are shown in Figure 2. The details of the model are summarized in Table I. In model #1, no n^+/n^{++} regions are formed and SR is neglected while the bulk lifetime is varied to clarify only the effect of the bulk lifetime. In this case, the base saturation current density (J_0) is set to match with the experimental V_{oc} for 5.6 Ω cm substrate. In model #2, the n^+/n^{++} regions are formed, but constant bulk lifetime, to observe the effect of n^+/n^{++} and SR. In model #3, n^+/n^{++} regions are formed and bulk lifetime are varied. The base parameters for n^+/n^{++} and the substrate used for the calculation for models #1–#3 are summarized in Table II. They are basically derived from the actual cell structure in

TABLE I. Summary of the calculated models.

Model	Considering n^+/n^{++}	Bulk lifetime (ms)	Considering SR	Structure
#1	No	0.23–1.0	No	Fig. 2(b)
#2	Yes	1.0 (constant)	Yes	Fig. 2(a)
#3	Yes	0.65–1.0	Yes	Fig. 2(a)

TABLE II. Basic parameters used for the calculation.

Region	Width (μm)	Doping concentration (cm^{-3})	Recombination velocity (cm/s)	Thickness (μm)
n^+ region	1300	1×10^{19}	200	0.15
n^{++} region	200	5×10^{19}	200	0.15
Substrate	1500	8×10^{14}–9×10^{15}	...	200

the experiment. For models #2 and #3, the n^{++} FSF region is formed for a metal contact. The n^{++} region and the front grid have a width of 200 μm and 80 μm, respectively. The substrate thickness is 200 μm. The differences between the experimental and calculated cell structure are a surface morphology and FSF doping profile. The surface morphology of the experimental cell has random pyramids but it is flat in the calculated model to reduce a computation time. Also in the experimental cell, the shape of the grids and the existence of bus bars make the practical shadow area different from the calculated model. Therefore, we use the experimentally measured reflectance of the cell for the wavelength in the range of 300–950 nm in the calculation. The wavelength of over 950 nm cannot be calculated accurately in the simulator. However, we found that the experimental QE curves of over 950 nm shows little difference in all cases because the J_{sc} loss is mainly due to the short to medium wavelength region, as shown in Figure 1(b). The maximum error would be around 0.1 mA/cm^2, similar to the measurement error. Therefore, we do not need the accurate calculation for the wavelength region over 950 nm to estimate J_{sc} loss. We calculate the contribution of the long wavelength region to J_{sc} from the experimental QE and the reflectance curve. Also, we multiplied the constant coefficient, which corresponds to the actual aperture ratio, to match with J_{sc} for the substrate with a high resistivity, where the J_{sc} loss becomes a minimum (shown later). The depth profile of the phosphorus at the n-type doping region is unclear for the experimental cell due to the textured surface. Therefore, we use the uniform phosphorus doping profile with a specific depth to simplify. The phosphorus concentrations in an n^+ region and n^{++} region are 1×10^{19} and 5×10^{19} cm^{-3}, respectively. The depth is chosen as 150 nm both for n^+ and n^{++} regions so that the sheet resistance of the calculated cell becomes almost similar to that of the experimental cell. As a front and a rear side passivation layers for the calculated cell, we have added the SiN layer. In case, we use the different structure or the parameters for the calculation, we specify the difference for each case. For the recombination model, we use Shockley-Read-Hall (SRH) and Auger recombination model.[18] For models #2 and #3, the surface recombination velocity is kept at constant for each surface except for the electrode area, where the recombination velocity is in the order of 10^4 cm/s. The recombination velocity for the front surface is chosen as 200 cm/s to achieve a reasonable V_{oc}, similar to the experiment. The bulk lifetime is one of the important parameters for the calculation; it is varied depending on the condition of the calculation. The bandgap narrowing is also considered using Schenk's model.[19] The carrier mobility is varied by the doping concentration and the device temperature is 298 K for calculation, as well as for the experimental measurement.

III. RESULTS AND DISCUSSION

A. Comparison between experiment and calculation for RE Si solar cell

Figure 3 shows the experimental data for the RE cell as a function of the resistivity of the Si substrate. The V_{oc} was almost constant or might slightly decrease with the decrease in the resistivity, but still the change is less than 0.5%. In

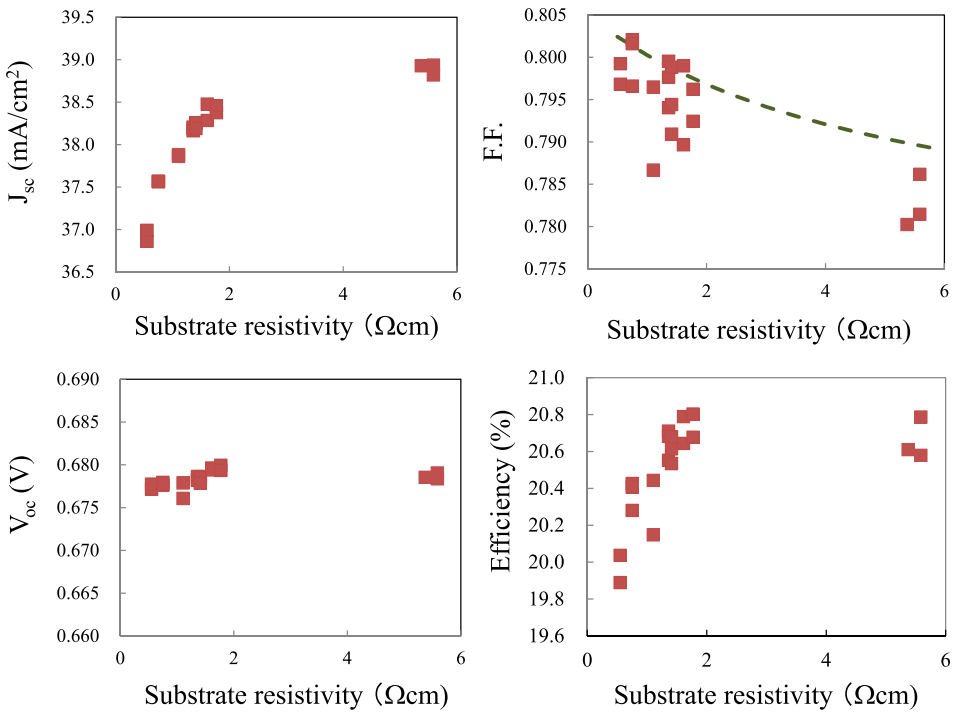

FIG. 3. Solar cell performance of the rear emitter cell as a function of the substrate resistivity. A dashed line in F.F. indicates the calculated data considering a series resistance which includes a sheet resistance of the n^+ doped region and the substrate.

contrast, F.F. decreased by increasing the resistivity. The change was around +2%. This is easily explained by the increase in series resistance due to the increase in sheet resistance of the substrate. The dashed line shows the calculated F.F. assuming the change in the sheet resistance due to the change in the resistivity of the wafer. The trend of the dashed line matches well with the experimental results. The variation for the F.F. even with the same resistivity shown here is mainly due to the variation in the grid resistance but this is out of scope for this paper.

The clear influence of the resistivity was also observed in J_{sc}. The J_{sc} decreased with the decrease in resistivity. The change in J_{sc} was nearly −5% in this resistivity range. Thus, the efficiency decreased from 20.8% to 20.1% (−3%) by decreasing the resistivity from 5.6 to 0.55 Ω cm. We have also done the experiment for the FE cell with the same resistivity range, but the change in J_{sc} caused by the low resistivity substrate was around −1%. Therefore, strong dependence of J_{sc} on the substrate resistivity is a more serious problem for the RE cell.

To explain this phenomenon, we first check the effect of the carrier lifetime of the substrate, assuming the variation of the lifetime is the main cause of the decrease in J_{sc}. Figure 4 shows the calculated J_{sc}, V_{oc}, and the lifetime of the substrate used in the calculation. In this calculation, we use model #1 as shown in Table I to observe the effect of the bulk lifetime. We assume that the lifetime of the substrate with the highest resistivity is 1 ms, which is a reasonable value from the lifetime measured after the high temperature processes. Then the bulk lifetime of the other substrate with a different resistivity used for the calculation is chosen to match with the experimental J_{sc}.

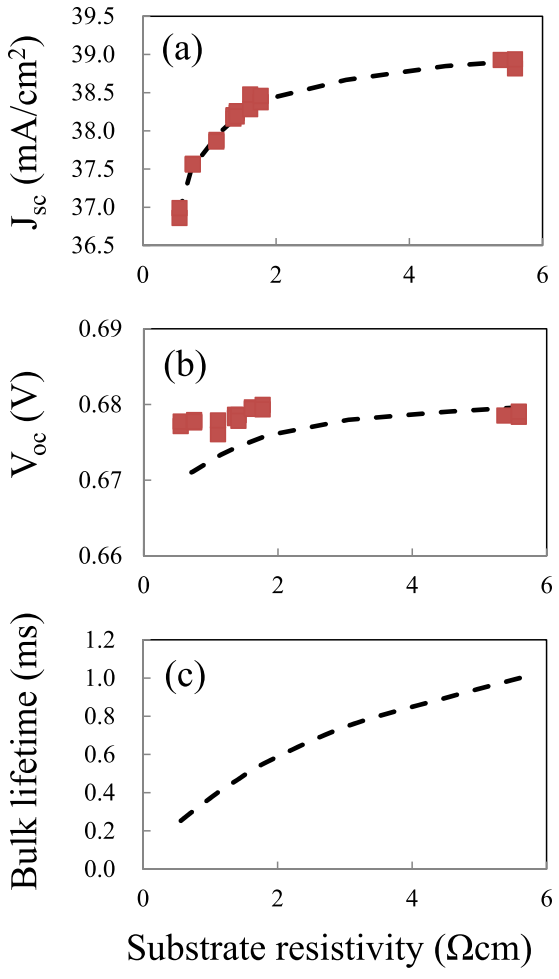

FIG. 4. Measured (red square) and calculated (dashed line) (a) J_{sc} (b) V_{oc} and (c) bulk lifetime used for the calculation as a function of the substrate resistivity. In this calculation, the effect of FSF and the surface recombination is neglected to observe only the bulk lifetime effect.

The similar trends of J_{sc} can be obtained by decreasing the lifetime from 1 ms down to 0.23 ms as a minimum for the lowest resistivity. The decrease of J_{sc} is attributed to the decrease of the diffusion length L, which depends on the carrier lifetime and the diffusion coefficient (or mobility). Since the change in the diffusion coefficient in this resistivity range is small (∼10%), the main cause is the decrease in the lifetime. It is clear that the low lifetime causes the low J_{sc}. In case the bulk lifetime is low, J_{sc} would be strongly affected by the recombination loss in the substrate. However, the calculated V_{oc} shows the noticeable decrease in contrast to the experimental results in our case. The decrease in V_{oc} is of course caused by the increase of J_0: increased carrier recombination by reduced L in the substrate. This data shows that the recombination in the bulk substrate may not be the major cause of the J_{sc} loss for the RE cell with a low resistivity substrate.

Then, we calculate the I-V characteristics using the structure model with n^+ and n^{++} doping regions on the front side (model #2). In this case, the bulk lifetime is kept as 1 ms as constant for all substrates, regardless of the resistivity. Figure 5 shows the calculated J_{sc} and V_{oc}. In this case, the trend of the J_{sc} loss is also similar as the experimental results. In addition, the calculated V_{oc} shows only small changes. By looking closer to the calculated V_{oc}, we found that it slightly increases by decreasing the resistivity of the substrate below 1 Ω cm. We will discuss about V_{oc} later. Since the structural difference between the previous and this model is the existence of n^+ and n^{++} regions, the J_{sc} loss in this calculation would be due to the recombination at the highly doped region (auger recombination) and the surface.

From the calculation, we found both the auger recombination and the surface recombination are important to reproduce the experimental data. To explain the mechanism of the J_{sc} loss, here we take the auger recombination in FSF as an example. In Table III, the details of calculated J_{sc} loss by the auger recombination in the FSF region are shown. In addition, the average hole concentration in each region is shown. For the cell with a high resistivity, the auger recombination loss is small; therefore, the main J_{sc} loss is caused by the SRH recombination in the substrate. The significant loss of J_{sc} by the auger recombination is observed for lower resistivity (0.55 Ω cm) substrate. The J_{sc} loss by the auger recombination in the n^{++} region is almost similar as in the n+ region, even though the surface area of n^{++} region is 13% of the whole area and less minority carrier (hole) in n^{++} region due to the higher FSF effect. The auger recombination rate is approximately proportional to the square of the majority carrier concentration in the FSF region. Five times higher

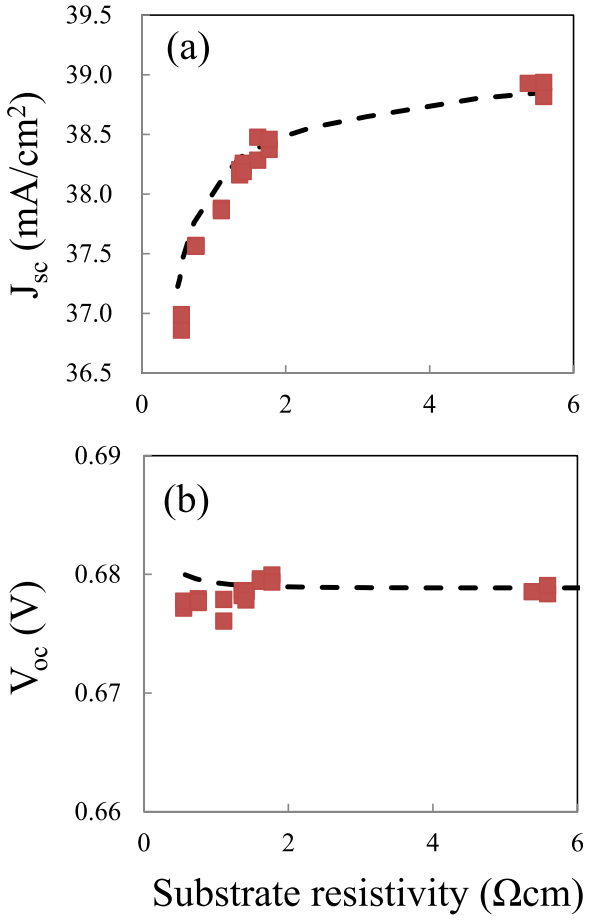

FIG. 5. Measured (red square) and calculated (dashed line) (a) J_{sc} and (b) V_{oc} as a function of the substrate resistivity. The bulk lifetime is kept constant as 1 ms. FSF is included and the surface recombination is considered.

electron concentration in the n^{++} region than in the n^{+} region causes the J_{sc} loss even higher.

As shown in Table III, the calculated J_{sc} loss by auger recombination in the n^{+} region becomes 3.8 times and 8.3 times higher for the substrate resistivity of 1.2 and 0.55 Ω cm, compared to that of 5.6 Ω cm. Since the auger recombination is also proportional to the minority carrier concentration, the increase in the hole concentration in the n^{+}/n^{++} regions by reducing the substrate resistivity should be matched with the increase in the auger recombination loss. The hole concentration in the FSF region (n^{+} or n^{++}) can be easily estimated from the hole concentration in the substrate and the barrier height φ_b at the valence band between the substrate and FSF doping region, as shown in the following equations:

$$\varphi_b = E_{v_{sub}} - E_{v_{n+}} = E_{f_{n+}} - E_{f_{sub}} - 1/2\Delta E_{bgn} \approx \frac{kT}{q}\ln\left(\frac{N_{d_{n+}}}{N_c}\right) - \frac{kT}{q}\ln\left(\frac{\Delta p + N_{d_{sub}}}{N_c}\right) - \Delta E_{bgn}, \quad (1)$$

where E_v is the energy of the valence band for each region, E_f is the fermi level for the electron, Δp is an average minority carrier concentration in the substrate near FSF, N_{dsub} is the doping concentration for the bulk, N_c is the effective density of state in conduction band, ΔE_{bgn} is the barrier lowing due to the band gap narrowing effect, k is a Boltzmann constant, T is a device temperature, and Δp is around 3–4 × 10^{14} cm^{-3} in this condition. The reduction of barrier height is, for example, 0.035 eV by increasing the substrate resistivity from 5.6 Ω cm to 1.2 Ω cm. This reduction in the barrier height should increase the minority carrier concentration in the FSF region by 3.8 times, as shown in Table III. Then it leads to the increase in the J_{sc} loss by 3.8 times. For n^{+} region, the result matches well with the increase in the hole concentration and the auger recombination. Therefore, the change in the barrier height between the FSF region and the substrate is the dominant factor for J_{sc} loss in this case.

For the low resistivity wafer, around half of the total J_{sc} loss is due to the SRH recombination, which are the surface and the bulk recombination. The same logic can be applied to the analysis of J_{sc} loss by the surface recombination because it is also proportional to the minority carrier density in FSF. For example, the J_{sc} losses due to SR passivated by SiN region are 0.03, 0.13, and 0.28 mA/cm^2 for 5.6, 1.2, and 0.55 Ω cm wafers, respectively, in our calculation. Their ratios are similar to the auger recombination loss as shown in Table III. For n^{++} region, the trend is similar but there is a slight deviation for the hole concentration from what we expect from the barrier height. This is caused by the shadowing effect by the electrode; there is no carrier generation below the electrode. The carriers diffuse into this region where no generation occurs, and the average hole concentration decreased from what is expected.

The FE cell shows less dependence of J_{sc} on the substrate resistivity. The reason is the difference in generation profile of the carriers in the substrate. For the RE cell, the light enters from the FSF side, therefore the most carriers are generated near the FSF surface. On the other hand, the light enters from the emitter side for the FE cell so that the most

TABLE III. Summary of the J_{sc} loss by the auger recombination in n^{+} and n^{++} regions. Hole concentration is derived from the simulator and the barrier height derived from Equation (1) is also shown. Each value is normalized based on the corresponding value for the substrate resistivity of 5.6 Ω cm.

Substrate resistivity (Ω cm)	N_{dsub} (cm^{-3})	Region	Hole concentration (cm^{-3})	Hole concentration Normalized	Auger recombination loss (mA/cm^2)	Auger recombination loss Normalized	$\emptyset_b$ (eV)	$\exp\left(\frac{\emptyset_{b5.6}-\emptyset_b}{kT}\right)$
5.6	8×10^{14}	n^{+} region	1.2×10^{12}	1.0	0.05	1.0	0.147	1.0
1.2	4×10^{15}		4.5×10^{12}	3.8	0.20	3.8	0.112	3.8
0.55	9×10^{15}		9.6×10^{12}	8.3	0.44	8.3	0.093	8.2
5.6	8×10^{14}	n^{++} region	4.4×10^{11}	1.0	0.07	1.0	0.165	1.0
1.2	4×10^{15}		1.7×10^{12}	3.9	0.27	3.9	0.129	4.0
0.55	9×10^{15}		3.5×10^{12}	8.0	0.56	8.0	0.109	8.7

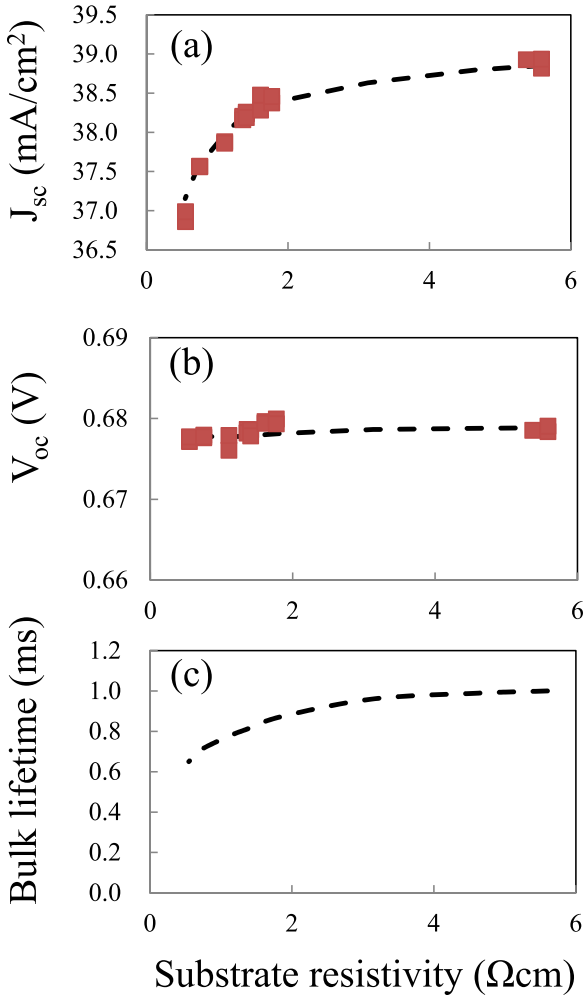

FIG. 6. Measured (red square) and calculated (dashed line) (a) J_{sc} and (b) V_{oc} as a function of the substrate resistivity. The lifetime used for the calculation varies with the substrate resistivity as shown in (c) to match with experimental V_{oc}.

carriers are generated near the emitter. This difference causes the large difference in the hole concentration near FSF. The hole concentration in the substrate region for the RE cell (when $V = 0$) is in the order of $10^{14}\,cm^{-3}$, while it is in the order of 10^{13} cm^{13} for the FE cell. Thus, the recombination loss in FSF is smaller for the FE cell than for the RE cell.

The bulk lifetime is still important to explain the V_{oc}. Previous calculation shows a slight gap in V_{oc}; in the experiment, we observe almost constant $V_{oc,}$ but V_{oc} increases with the decreasing resistivity in the calculation. This result can be explained by the decrease of the bulk lifetime. Figure 6 shows the calculated J_{sc}, V_{oc}, and the bulk lifetime as a function of the substrate resistivity, using model #3. The bulk lifetime is chosen to match V_{oc}. The slight change in the bulk lifetime causes the calculated V_{oc} to match with the experimental value. Since the bulk lifetime is over 0.65 ms for all the substrates, the additional J_{sc} loss is limited to 0.2–0.3 mA/cm^2 or less even at the lowest bulk lifetime. The both calculated V_{oc} and J_{sc} match better with the experimental data by using model #3.

The increase in the J_{sc} loss in the RE cell denotes the decrease in the hole concentration. Therefore, it seems reasonable that a change in the substrate resistivity leads to the large drop of hole concentration and non-negligible decrease of V_{oc} at the same time. However, both the experimental and the calculated results show almost no change in V_{oc}. The V_{oc} is equal to a difference between the quasi-fermi level of electron and hole when $J = 0$; therefore, it can be calculated using Δp and N_{dsub} as shown in the following equation:[20]

$$V_{oc} = \frac{kT}{q}\ln\left(\frac{(\Delta p + N_{d_{sub}})\Delta p}{{n_i}^2}\right), \tag{2}$$

where n_i is the intrinsic carrier concentration. The minority carrier concentration in the substrate decreases from around $4 \times 10^{15}\,cm^{-3}$ to $2 \times 10^{15}\,cm^{-3}$ by decreasing the substrate resistivity from 5.6 Ω cm to 0.55 Ω cm, including the effect of the change in the bulk lifetime. The reduction of the hole concentration itself leads to around 15 mV reduction of V_{oc}. On the other hand, the increase of N_d causes the fermi level of electron to be 13–14 mV higher. (The electron concentration increases from around 5×10^{15} to $1 \times 10^{16}\,cm^{-3}$, by decreasing the resistivity, including the electron generated by the light.) This increment cancels the effect of the reduction of the minority carrier concentration in the substrate. As a result, the reduction of V_{oc} is limited to a few mV. It also can be explained by the change in a reverse saturation current density (J_0).[21] J_0 due to the recombination of FSF ($J_{0,FSF}$) and the bulk ($J_{0,bulk}$) was experimentally evaluated and they were around $5–6 \times 10^{-14}$ and $3–4 \times 10^{-14}$ A/cm^2, respectively, for the substrate resistivity of 1.2 Ω cm. By increasing the resistivity from 1.2 Ω cm to 5.6 Ω cm, $J_{0,FSF}$ would decrease to $3–4 \times 10^{-14}$ A/cm^2 (or become 2/3) because the barrier height for the hole would be higher by ~10 mV at V_{oc} condition. On the other hand, $J_{0,bulk}$ would be increased to $4–5 \times 10^{14}\,A/cm^2$ due to the increase in the minority carrier concentration in the bulk. Therefore, the summation of $J_{0,FSF}$ and $J_{0,bulk}$ was almost similar even the resistivity of the substrate is different. Therefore, V_{oc} is similar for different resistivities in the range between 0.55 and 5.6 Ω cm, as shown in the previous calculation. If the bulk lifetime is much lower for the substrate with the lower resistivity as shown in Figure 4, or the surface recombination velocity is higher, then they result in a large drop of V_{oc} due to the increase in $J_{0,bulk}$ or $J_{0,FSF}$.

These results indicate that the significant J_{sc} loss by FSF can be occurred even without the drop in the bulk lifetime. Since V_{oc} strongly depends on the bulk lifetime, the reason for the drop of J_{sc} can be judged by monitoring V_{oc}: if V_{oc} drops by varying the substrate resistivity, then the bulk lifetime would be one of the reasons that decrease J_{sc}.

B. Reduction of J_{sc} loss

From Sec. III A, we know that the substrate with a higher resistivity will help to achieve the higher J_{sc} for the RE cell because of the higher barrier height. But still it is important to discuss other ways to reduce the J_{sc} loss because the resistivity of the wafers would be varied even within the same ingot for n-type doped Si. There would be several ways:

(1) Reduction in the wafer thickness
(2) Reduction in the doping concentration in FSF

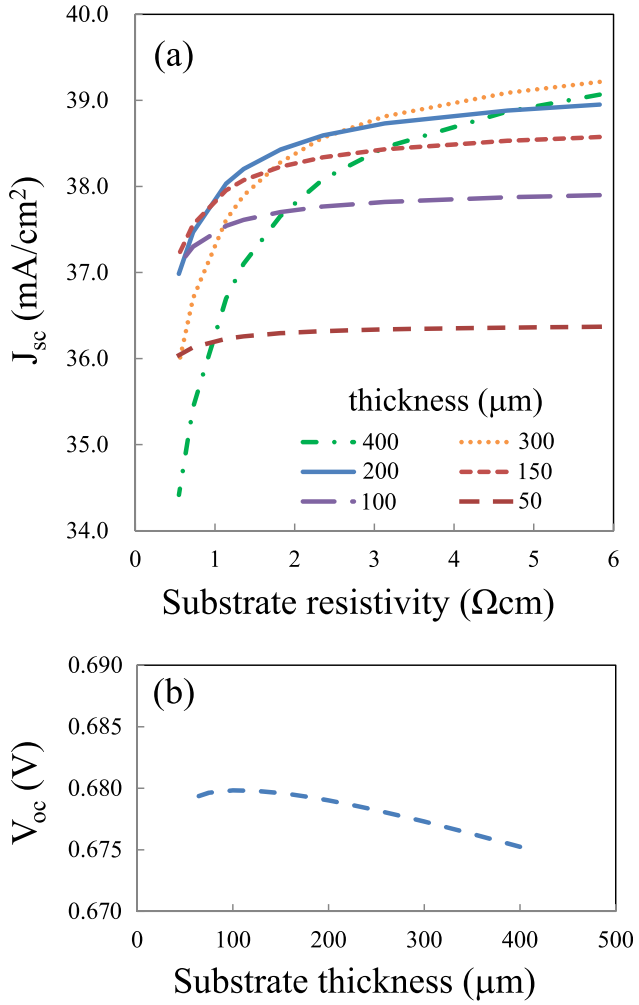

FIG. 7. Calculated (a) J_{sc} and (b) V_{oc} as a function of the substrate resistivity and the thickness. The thickness is varied from 50 to 400 μm. The parameters used for the calculation are shown in Table I. The bulk lifetime is varied according to the result shown in Fig. 6. V_{oc} is calculated for the substrate resistivity of 1.2 Ω cm.

(3) Increase in barrier height for the minority carrier between FSF and the substrate.

The following data are the calculated results which show the effect of the methods listed above.

The reduction of the wafer thickness will reduce the J_{sc} loss at FSF, as explained in Sec. III A, but still there is another negative impact. Figure 7 shows the dependence of calculated (a) J_{sc} on the resistivity and the thickness and (b) V_{oc} on the thickness of the substrate. The calculated maximum J_{sc} for the thin wafer (<=100 μm) may contain errors due to the lack of data for estimating the behavior of the long wavelength region, but still the trend is clearly observed because the J_{sc} loss mainly occurs at the short to medium wavelength region. As shown here, the J_{sc} depends less on the resistivity for the thinner substrate. The electrical field by the emitter can pump the minority carriers out from the substrate more efficiently and decrease the J_{sc} loss at FSF. On the other hand, the thinner substrate absorbs less light, especially the light with the long wavelength. As a result, the maximum J_{sc} is reduced. The thinner wafer achieves higher V_{oc} due to the higher generation density in the bulk

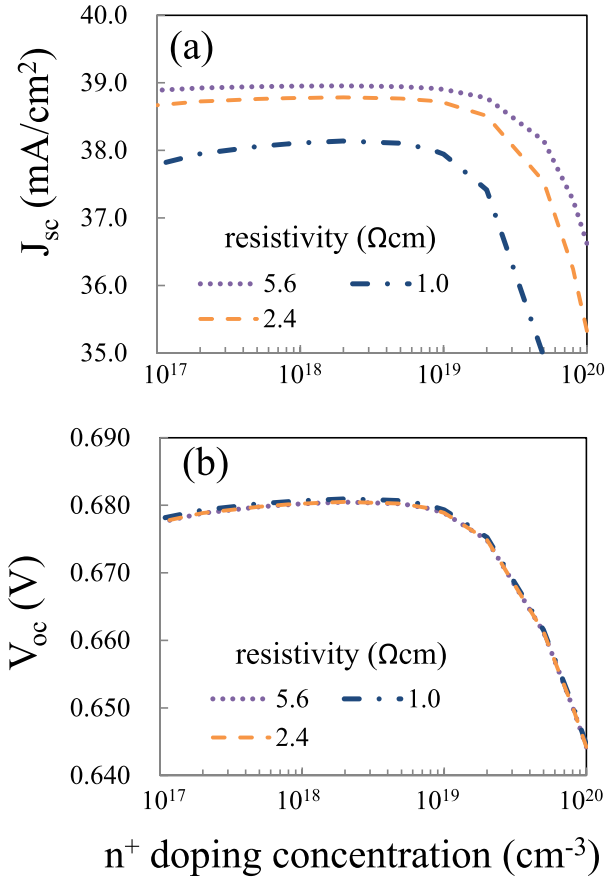

FIG. 8. Calculated (a) J_{sc} and (b) V_{oc} as a function of the substrate resistivity and doping concentration in the n^+ region. The parameters used for the calculation are shown in Table I. The bulk lifetime is varied according to the result shown in Fig. 6.

substrate, as reported elsewhere.[22,23] However, the effect of the surface recombination is also enhanced with thinner substrate and V_{oc} starts decreasing below a certain thickness, which depends on the surface recombination velocity. Therefore, a restriction of the surface recombination is mandatory. Furthermore, if the transmittance and reflection loss are reduced by the efficient optical design, such as inverted pyramid structure with anti-reflection coating, then the J_{sc} loss would be less and the efficiency would be improved even with the thinner wafer.

Reduction of the doping concentration in FSF will reduce the auger recombination loss. In contrast, the barrier height for the minority carriers decreases and the effect of the surface recombination velocity increases. Figure 8 shows the dependence of J_{sc} and V_{oc} on the doping level in n^+ region. The small improvement of J_{sc} can be obtained by decreasing the doping level down to 10^{18} cm^{-3}. The auger recombination becomes less by the reduction of the electron density at FSF. However, the surface recombination rate will increase in this case. Lower than 10^{18} cm^{-3} causes the J_{sc} drops as well as V_{oc}. Lowering doping concentration decreases the barrier height at the valence band, and the hole concentration at the surface of the cell increases, resulting in the increase of the surface recombination rate. The use of the substrate with the resistivity less than 1 Ω cm would be difficult to achieve high J_{sc}. A more effective way is to control

the n^{++} region. There is the n^{++} region in our cell to reduce the contact resistance and restrict the surface recombination by the electrode. The width of the n^{++} region is wider than the electrode to make the alignment easier for the screen printing. The J_{sc} loss due to this extra region reaches to around 20% (around 0.3–0.4 mA/cm^2 for the substrate resistivity of 0.55 Ω cm) of the total J_{sc} loss. Minimizing the width of the n^{++} region will improve J_{sc} as well as V_{oc}. These results also relate to an interdigitated back contact solar cell, which has both electrode contacts on the rear side. If the FSF region is highly doped, then the J_{sc} loss dependence on the resistivity of the wafer becomes significant. But principally it does not require the n^{++} region on the front side since all the contacts are located on the rear side. Therefore, it has the great advantages for the reduction of J_{sc} loss by keeping the doping concentration less than $10^{19}\,cm^{-3}$.

The increase in the barrier height will improve the performance of the cell without any degradation. Therefore, it is the ultimate way to solve the problem. Figure 9 shows the dependence of the calculated J_{sc} on the barrier height. In this calculation, the energy level of the valence band for FSF layer and the resistivity of the substrate are varied. The substrate thickness is 200 μm and the doping concentration at FSF is kept as $1 \times 10^{19}\,cm^{-3}$. To confirm only the effect of the barrier height, the bulk lifetime is kept high to eliminate the effect of the bulk recombination loss. The optical bandgap is kept the same as Si, so the generation rate in the cell is the same in all conditions. As shown in the figure, J_{sc} is not the function of the resistivity anymore but the function of the barrier height. The barrier height lower than 0.1 eV drastically decrease J_{sc}. When the barrier height is above 0.2 eV, then J_{sc} saturates and no resistivity dependence is practically observed. This result also indicates that the resistivity itself is not the point but the barrier height is a key point to explain the J_{sc} loss shown in Figure 3. The inset of Figure 9 shows the J_{sc} loss in FSF based on the saturated J_{sc} as a function of barrier height. The J_{sc} loss by the auger recombination can be also calculated with the minority carrier concentration in FSF

$$J_{loss\_auger} \sim qdC_n {n_{FSF}}^2 p_{sub} \exp\left(-\frac{q\varphi_b}{kT}\right), \qquad (3)$$

where C_n is the auger recombination coefficient, n_{FSF} is an electron concentration, p_{sub} is the hole concentration in the substrate near the FSF region, d is the thickness of the FSF region. A dashed line in the inset of Figure 9 shows the calculated data using Equation (3). The gradient of the dashed line matches well with data calculated by the device simulator. The dashed line is slightly shifted from the data calculated by the device simulator because Equation (3) does not include the loss by SRH recombination at the surface. The J_{sc} loss would be shifted from the guided line calculated by Equation (3) when the lifetime is smaller or the substrate is thinner; the diffusion of the carriers would play an important role in that case.

It is difficult to achieve the barrier height higher than 0.2 eV for the homojunction cell, especially for a high V_{oc} cell. However the band gap engineering is possible for the heterojunction cell to reduce the resistivity dependence.

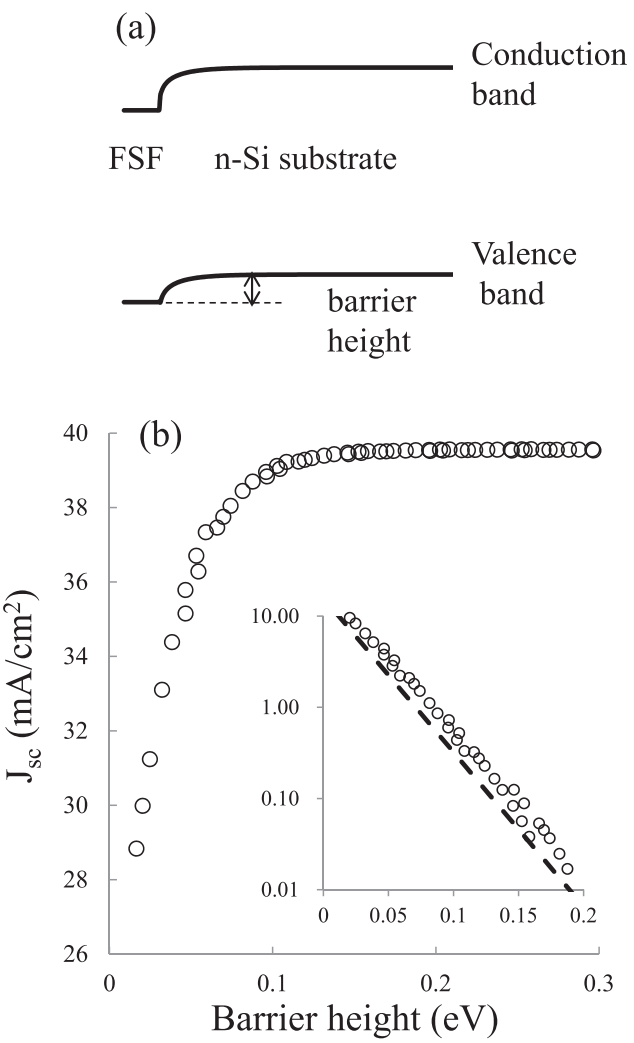

FIG. 9. (a) Energy band diagram for FSF/n-Si substrate and (b) calculated J_{sc} as a function of the barrier height for the minority carriers. The resistivity and the bandgap (E_g) for FSF is varied simultaneously while the work function remains constant. The resistivity is varied from 0.55 to 5.6 Ω cm. The bandgap of FSF is varied from $E_g - 0.1$ eV to $E_g + 0.15$ eV. Only the loss in the n^+ region is considered for the calculation of J_{sc}. The effect of the n^{++} region and the bulk lifetime is neglected. The inset shows the J_{sc} loss as a function of a barrier height. The dashed line is a guide line, which is calculated with $qdC_n{n_{FSF}}^2 p_{sub}\exp(-q\varphi_b/kT)$, where C_n ($2.2 \times 10^{-31}\,cm^{-6}/s$) is an auger recombination coefficient, n_{FSF} is the electron concentration ($1 \times 10^{19}\,cm^{-3}$) in the n^+ region, p_{sub} is an average hole concentration ($\sim 3 \times 10^{14}\,cm^{-3}$) in a substrate near FSF, and d is a width of n^+ layer (150 nm).

Figure 10 shows the experimental results for the heterojunction rear emitter cell. Details of the cell structure are given in Ref. 5. J_{sc} itself is not so high as the homojunction cell because of the thinner wafer (<150 μm) and UV absorption by a window layer (microcrystalline and amorphous Si). Still, the J_{sc} trend clearly indicates that J_{sc} does not depend on the resistivity of the substrate for the heterojunction solar cell. The heterojunction solar cell has a long lifetime (>3 ms) because of the low temperature process. In addition, the wafer thickness is thinner so that the effect of the diffusion length is negligible. The auger recombination as well as the surface recombination is not the problem because an intrinsic layer has no doping and the barrier height more than 0.5 eV. V_{oc} as high as 0.740 V shows the very low

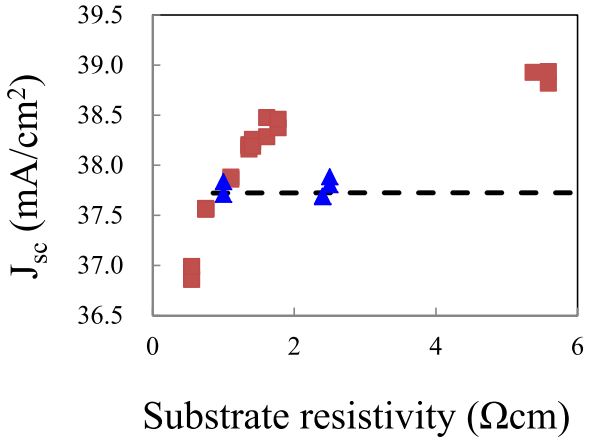

FIG. 10. The measured J_{sc} (blue triangle) for the rear emitter heterojunction Si solar cell. Red square is the data for the rear emitter homojunction cell with FSF. The dashed line indicates the calculated J_{sc} considering the barrier height and the substrate thickness for the heterojunction cell. The V_{oc} of the heterojunction cell is around 0.740 V.

recombination rate near at FSF. The absorption loss for the short wavelength at the n-layer also helps the distribution of the generation rate within the substrate to shift toward the emitter, results in the transport of minority carriers to the emitter more effectively. Therefore, the heterojunction solar cell possesses all the features listed previously to reduce the J_{sc} loss caused by the resistivity variation.

IV. CONCLUSION

The dependence of J_{sc} loss on the base resistivity of the substrate is analyzed by 2D device simulator and compared with the experimental results. V_{oc} does not show the clear dependence on the resistivity in the range of 0.55–5.6 Ω cm. On the other hand, J_{sc} strongly depends on the barrier height between FSF and the substrate for the minority carriers. The substrate with a higher resistivity produce a higher surface field effect, thus it brings higher J_{sc}. The lower substrate resistivity leads to lower barrier height, thus the J_{sc} loss is high because of the auger recombination and the surface recombination. The control of the doping concentration in FSF is very important to minimize the J_{sc} loss in FSF. The thinner wafer with proper optical trapping also helps to reduce the J_{sc} loss. Furthermore, the passivation layer with a wide bandgap, such as amorphous Si layer, enables to reduce the J_{sc} loss at FSF drastically.

ACKNOWLEDGMENTS

The authors would like to thank Dr. Shinsuke Miyajima, Associate Professor in Tokyo Institute of Technology, for the fruitful discussions and valuable suggestions. A part of this work was supported by the New Energy and Industrial Technology Development Organization (NEDO).

[1]L. J. Geerligs, P. Manshanden, I. Solheim, E. J. Ovrelid, and A. N. Waernes, in *Proceedings of the 21st European Photovoltaic Solar Energy Conference and Exhibition* (2006), p. 1285.
[2]A. Edler, J. Jourdan, V. D. Mihailetchi, R. Kopecek, R. Harney, D. Stichtenoth, T. Aichele, A. Grochocki, and J. Lossen, in *Proceedings of the 25th European Photovoltaic Solar Energy Conference and Exhibition* (2010), p. 1905.
[3]S. Nishimura, T. Watahiki, D. Niinobe, T. Hayashida, Y. Yuda, S. Kano, K. Nishimura, H. Tokioka, and M. Yamamuka, "Over 21% Efficiency of n-Type Monocrystalline Silicon PERT Photovoltaic Cell With Boron Emitter," IEEE J. Photovoltaics (to be published).
[4]M. Taguchi, A. Yano, S. Tohoda, K. Matsuyama, Y. Nakamura, T. Nishiwaki, K. Fujita, and E. Maruyama, IEEE J. Photovoltaics **4**, 96 (2014).
[5]T. Watahiki, T. Furuhata, T. Matsuura, T. Shinagawa, Y. Shirayanagi, T. Morioka, T. Hayashida, Y. Yuda, S. Kano, Y. Sakai, H. Tokioka, Y. Kusakabe, and H. Fuchigami, Appl. Phys. Express **8**, 021402 (2015).
[6]E. Kobayashi, N. Nakamura, K. Hashimoto, and Y. Watabe, in *Proceedings of the 28th European Photovoltaic Solar Energy Conference and Exhibition* (2013), p. 691.
[7]M. Bivour, S. Schröer, M. Hermle, and S. W. Glunz, Sol. Energy Mater. Sol. Cells **122**, 120 (2014).
[8]A. Uruena de Castro, M. Aleman, E. Cornagliotti, A. Sharma, J. Deckers, M. Haslinger, L. Tous, R. Russell, J. John, Y. Yao, T. Söderström, F. Duerinckx, and J. Szlufcik, in *Proceedings of the 31st European Photovoltaic Solar Energy Conference and Exhibition* (2015), p. 410.
[9]V. Mertens, T. Ballmann, J. Y. Lee, M. Junghänel, F. Stenzel, L. Brandt, A. Schulze, P. Engelhart, J. W. Müller, P. Wawer, and K. H. Küsters, Energy Procedia **27**, 53 (2012).
[10]T. Ballmann, V. Mertens, C. Peters, M. Koentopp, J. Cieslak, A. Schonmann, C. Klenke, M. Kauert, G. Zimmermann, S. Bordihn, and J. W. Muller, Energy Procedia **55**, 396 (2014).
[11]A. ur Rehman and S. H. Lee, Sci. World J. **2013**, 470347.
[12]M. Hermle, F. Granek, O. Schultz, and S. W. Glunz, J. Appl. Phys. **103**, 054507 (2008).
[13]M. Bivour, M. Rüdiger, C. Reichel, K.-U. Ritzau, M. Hermle, and S. W. Glunz, Energy Procedia **8**, 185 (2011).
[14]F. Book, T. Wiedenmann, G. Schubert, H. Plagwitz, and G. Hahn, Energy Procedia **8**, 487 (2011).
[15]S. Bordihn, V. Mertens, P. Engelhart, T. Florian, J. Cieslak, F. Stenzel, P. Kappe, T. Ballmann, J. Y. Lee, T. Lindner, M. Junghanel, J. W. Muller, W. M. M. Kessels, and P. Wawer, in *Proceedings of the 26th European Photovoltaic Solar Energy Conference* (2011), p. 429.
[16]Y. Schiele, F. Book, S. Seren, G. Hahn, and B. Terheiden, Energy Procedia **27**, 460 (2012).
[17]User Manual of Silvaco ATLAS, Software Version 5.18.3.R, 2012.
[18]M. J. Kerr and A. Cuevas, J. Appl. Phys. **91**, 2473 (2002).
[19]A. Schenk, J. Appl. Phys. **84**, 3684 (1998).
[20]R. A. Sinton and A. Cuevas, Appl. Phys. Lett. **69**, 2510 (1996).
[21]D. E. Kane and R. M. Swanson, in *Proceedings of the 18th IEEE Photovoltaic Specialists Conference* (1985), p. 578.
[22]L. Wang, A. Lochtefeld, J. Han, A. P. Gerger, M. Carroll, J. Ji, A. Lennon, H. Li, R. Opila, and A. Barnett, IEEE J. Photovoltaics **4**, 1397 (2014).
[23]M. Taguchi, Y. Tsunomura, H. Inoue, S. Taira, T. Nakashima, T. Baba, H. Sakata, and E. Maruyama, in *Proceedings of the 24th European Photovoltaic Solar Energy Conference* (2009), p. 1690.